Direct Differentiation of the Particle Finite-Element Method for Fluid–Structure Interaction

Minjie Zhu[1] and Michael H. Scott, M.ASCE[2]

Abstract: Sensitivity analysis of fluid–structure interaction (FSI) provides an important tool for assessing the reliability and performance of coastal infrastructure subjected to storm and tsunami hazards. As a preliminary step for gradient-based applications in reliability, optimization, system identification, and performance-based engineering of coastal infrastructure, the direct differentiation method (DDM) is applied to FSI simulations using the particle finite-element method (PFEM). The DDM computes derivatives of FSI response with respect to uncertain design and modeling parameters of the structural and fluid domains that are solved in a monolithic system via the PFEM. Geometric nonlinearity of the free surface fluid flow is considered in the governing equations of the DDM along with sensitivity of material and geometric nonlinear response in the structural domain. The analytical derivatives of elemental matrices and vectors with respect to element properties are evaluated and implemented in an open source finite element software framework. Examples involving both hydrostatic and hydrodynamic loading show that the sensitivity of nodal displacements, pressures, and forces computed by the finite-difference method (FDM) converge to the DDM for simple beam models as well as for a reinforced-concrete frame structure. **DOI: 10.1061/(ASCE)ST.1943-541X.0001426.**

Author keywords: Particle method; Finite-element method; Sensitivity analysis; Fluid–structure interaction; Nonlinear analysis; Reliability analysis; Analysis and computation; OpenSees.

Introduction

Wave loads induced by tsunami and storm surge events can cause significant damage to critical coastal infrastructure as observed in recent natural disasters such as the 2011 Great East Japan earthquake and tsunami and the Superstorm Sandy hurricane of 2012 (Chock et al. 2013; McAllister 2014). Subsequent efforts to improve design and mitigation strategies for structures subject to similar hazards have increased efforts to refine fluid–structure interaction (FSI) simulation capabilities. The modeling of wave loads as static forces on a deformable body, or conversely as hydrodynamic forces on a rigid body, may not provide accurate predictions of structural response. To obtain accurate response for structural displacements and forces, fluid-–structure interaction must be considered accounting for the kinematics and deformation of both the structural and fluid domains. It is also imperative to assess the sensitivity of structural response to stochastic wave loading and uncertain structural properties. The sensitivity has important implications for the design of coastal infrastructure and in assessing the probability of failure of buildings and bridges in tsunami and storm events as part of an overarching performance-based engineering framework (Chock et al. 2011). Sensitivity analysis is also important for gradient-based applications such as reliability and optimization (Fujimura and Kiureghian 2007; Gu et al. 2012).

The simulation of fluid–structure interaction with incompressible Newtonian fluid is one of the most challenging problems in computational fluid mechanics because the incompressibility condition leads to numerical instability of the computed solution. A large number of finite-element methods (FEM) have been developed for the computation of incompressible Navier-Stokes equations using the Eulerian, Lagrangian, or Arbitrary Lagrangian-Eulerian (ALE) formulations (Girault and Raviart 1986; Gunzburger 1989; Baiges and Codina 2010; Radovitzky and Ortiz 1998; Tezduyar et al. 1992). The particle finite-element method (PFEM) (Oñate et al. 2004), has been shown to be an effective Lagrangian approach to FSI because it uses the same Lagrangian formulation as structures. A monolithic system of equations is created for the simultaneous solution of the response in the fluid and structural domains via the fractional step method (FSM). This alleviates the need to couple disparate computational fluid and structural modules through a staggered approach in order to simulate FSI response. Through the monolithic approach, compatibility and equilibrium are satisfied naturally along the interfaces between the fluid and structural domains.

While the solution of FSI simulations via a monolithic system has computational advantages in determining the structural response, the sensitivity of this response to uncertain design and modeling parameters is just as, if not more, important than the response itself. As a standalone product, sensitivity analysis shows the effect of modeling assumptions and uncertain properties on system response, but it is also an important component to gradient-based applications in reliability and optimization. There are two methods for calculating the sensitivity of a simulated response. The finite-difference method (FDM) repeats the simulation with a perturbed value for each parameter and does not require additional implementation as perturbations and differencing can be handled with preprocessing and postprocessing. The accuracy of the resulting finite-difference approximation depends on the size of the perturbation where the results are not accurate for large perturbations and are prone to numerical round-off error for very small perturbations. Due to the need for repeated simulations, the FDM approach can become inefficient when the model is large, which is

[1]Postdoctoral Researcher, School of Civil and Construction Engineering, Oregon State Univ., Corvallis, OR 97331. E-mail: zhum@oregonstate.edu

[2]Associate Professor, School of Civil and Construction Engineering, Oregon State Univ., Corvallis, OR 97331 (corresponding author). E-mail: michael.scott@oregonstate.edu

Note. This manuscript was submitted on December 31, 2014; approved on August 25, 2015; published online on November 4, 2015. Discussion period open until April 4, 2016; separate discussions must be submitted for individual papers. This paper is part of the ***Journal of Structural Engineering***, © ASCE, ISSN 0733-9445.

common for FSI simulations, and when there is a large number of parameters.

A more accurate approach to gradient computations is the direct differentiation method (DDM), where derivatives of the governing equations are implemented alongside the equations that govern the simulated response. At the one-time expense of derivation and implementation, as well as additional storage, the DDM calculates the response sensitivity efficiently as the simulation proceeds. This eliminates the need for the repeated simulations that are required for finite-difference calculation of the gradients. For a single parameter, the DDM generally requires one additional backward substitution to compute the sensitivity at a computational cost proportional to N^2, where N is the number of model degrees of freedom. Finite-difference methods (FDMs) require a full reanalysis to find the sensitivity with respect to each parameter at a cost proportional to N^3. For large models and/or models with a large number of parameters, the computational savings of the DDM over FDMs can be significant. The DDM is also more accurate than the FDM because the sensitivity is computed using the same numerical algorithm as the response, making it subject to only numerical precision rather than round-off error. Analytical approaches to DDM sensitivity analysis for structural response under mechanical loads have been well developed (Kleiber et al. 1997) and extended to material and geometric nonlinear formulations of frame-element response (Scott et al. 2004; Conte et al. 2004) as well as frame-element geometry and cross-section dimensions (Haukaas and Scott 2006; Scott and Filippou 2007). The DDM has also been applied to composites processing (Bebamzadeh et al. 2010) and fire attack on structures (Guo and Jeffers 2014); however, its application to FSI has not been addressed. This is partly due to the complexity of the computation for the FSI response and the cumbersome nature of staggered computational approaches.

The goal of this paper is to develop the DDM approach for computing the sensitivity of PFEM fluid–structure interaction simulations to uncertain design and modeling parameters of the fluid and structure domains. The PFEM response analysis will be introduced, including the governing equations, combined FSI discrete equations, and the fractional step method (FSM). Then, the DDM approach is applied to obtain the PFEM sensitivity equations for FSI, including geometrically nonlinear terms due to large displacements of the fluid particles. Examples include comparisons between DDM and FDM solutions for PFEM sensitivity in simple beam models, as well as applications to a prototypical coastal structure with nonlinear material and geometric response.

PFEM Response Computations

This section provides a brief review of the equations that govern FSI response using the PFEM. After applying finite-element techniques, discrete algebraic equations are formed from solid elements in the fluid domain and arbitrary line and solid elements in the structural domain. The algebraic equations will be differentiated in the following section for sensitivity analysis via the DDM. Although the presentation will focus on a particular fluid element, the methods described herein are generally applicable to any element formulation.

Governing Equations

All particles or nodes in the fluid and structural domains satisfy the governing differential equation of linear momentum

$$\rho \dot{v}_i = \frac{\partial \sigma_{ij}}{\partial x_j} + \rho b_i \tag{1}$$

where v_i = velocity vector; σ_{ij} = Cauchy stress tensor; x_j = current position vector; b_i = body acceleration vector; and ρ = solid or fluid density.

Mass conservation for incompressible fluid flow is described by the divergence of the velocity field being zero

$$\frac{\partial v_i}{\partial x_i} = 0 \tag{2}$$

The stress tensor can be decomposed into deviatoric and hydrostatic parts as

$$\sigma_{ij} = S_{ij} - p\delta_{ij} \tag{3}$$

where δ_{ij} = Kronecker delta; and p = fluid pressure. Assuming Newtonian flow, the constitutive equation for the fluid response is defined by

$$S_{ij} = 2\mu\dot{\varepsilon}_{ij} \tag{4}$$

where the deviatoric stress tensor S_{ij} is related to the strain rate $\dot{\varepsilon}_{ij}$ in the fluid by the viscosity μ.

Due to the inf-sup or Ladyzenskaja-Babuška-Brezzi (LBB) condition (Brezzi and Fortin 1991; Girault and Raviart 1986), for incompressible flow, the velocity and pressure spaces have to be modified in order to produce numerically-stable results. Donea and Huerta (2003) summarize stabilization approaches based on the use of bubble functions at the element level or artificial (penalty) parameters at the element or global levels. The classic PFEM uses the finite calculus method (FIC) to stabilize linear fluid elements (Oñate et al. 2006). In the literature, the bubble function and stabilized formulations have been shown to be equivalent (Bank and Welfert 1990; Matsumoto 2005; Pierre 1995).

MINI Element

The MINI element uses a bubble node for velocity at the element center of gravity to satisfy the inf-sup condition for incompressible fluids (Arnold et al. 1984). Although there are more accurate elements, the MINI element has been used in many fluid simulations (Lee et al. 2009; Gresho 1998) and it is easy to implement, making it an ideal choice to demonstrate the DDM for the PFEM. The element pressure field does not utilize the bubble node and is based on linear interpolation from the nodal pressures

$$p^e = N_1 p_1^e + N_2 p_2^e + N_3 p_3^e \tag{5}$$

where p_i^e = nodal pressures. The shape functions, N_i, are equal to the area coordinates, L_i, for any point in the triangle

$$N_i = L_i = \frac{A_i}{A}, \qquad i = 1, 2, 3 \tag{6}$$

The total area of the triangle is A, and A_i is the tributary area as shown in Fig. 1(a). The shape functions used for the 2D MINI element are similar to those used in a 3D formulation (Nakajima and Kawahara 2010). The Jacobian, J, that describes the element transformation from global coordinates to area coordinates is

$$J = x_2 y_3 - x_3 y_2 + x_3 y_1 - x_1 y_3 + x_1 y_2 - x_2 y_1 \tag{7}$$

where x_i and y_i = current coordinates determined from the current nodal displacements relative to the initial coordinates, x_i^0 and y_i^0, at the start of the simulation for each corner node

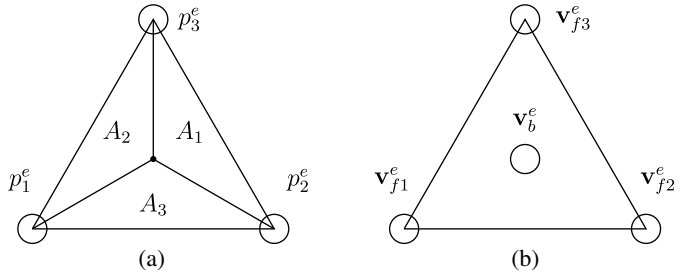

Fig. 1. Nodal unknowns for the MINI element: (a) pressure nodes; (b) velocity nodes

$$x_1 = x_1^0 + u_{f1}^e, \qquad x_2 = x_2^0 + u_{f3}^e, \qquad x_3 = x_3^0 + u_{f5}^e$$
$$y_1 = y_1^0 + u_{f2}^e, \qquad y_2 = y_2^0 + u_{f4}^e, \qquad y_3 = y_3^0 + u_{f6}^e \tag{8}$$

where u_{fk}^e = kth component of the displacement vector $\mathbf{u}_f^e$.

The fluid velocities, as shown in Fig. 1(b), are interpolated by

$$\mathbf{v}^e = N_1\mathbf{v}_{f1}^e + N_2\mathbf{v}_{f2}^e + N_3\mathbf{v}_{f3}^e + N_b\mathbf{v}_{f4}^e \tag{9}$$

where $\mathbf{v}_{f4}^e$ = nodeless variable defined as the difference between the bubble velocity and the average velocity of the nodes

$$\mathbf{v}_{f4}^e = \mathbf{v}_b^e - \frac{\mathbf{v}_{f1}^e + \mathbf{v}_{f2}^e + \mathbf{v}_{f3}^e}{3} \tag{10}$$

The shape function, N_b, applied to the nodeless velocity variable in Eq. (9) is defined in terms of the area coordinates

$$N_b = 27L_1L_2L_3 \tag{11}$$

Using the shape functions for pressure and velocity in the MINI formulation, the discrete equations for the fluid response at the element level are

$$\mathbf{M}_f^e\dot{\mathbf{v}}_f^e - \mathbf{G}_f^e\mathbf{p}^e = \mathbf{F}_f^e \tag{12}$$

$$\mathbf{M}_b^e\dot{\mathbf{v}}_{f4}^e - \mathbf{G}_b^e\mathbf{p}^e = \mathbf{F}_b^e \tag{13}$$

$$\mathbf{G}_f^{eT}\mathbf{v}_f^e + \mathbf{G}_b^{eT}\mathbf{v}_{f4}^e = \mathbf{0} \tag{14}$$

where $\mathbf{v}_f^e$ = velocity vector; $\mathbf{v}_{f4}^e$ is defined in Eq. (10); and $\mathbf{p}^e$ = pressure vector. The right-hand side contains viscous terms that have been combined with the external force vector

$$\mathbf{F}_f^e = \bar{\mathbf{F}}_f^e - \mathbf{K}_f^e\mathbf{v}_f^e \qquad \mathbf{F}_b^e = \bar{\mathbf{F}}_b^e - \mathbf{K}_b^e\mathbf{v}_b^e \tag{15}$$

For the MINI element with shape functions based on area coordinates, exact integration of the elemental matrices and vectors is possible. Using the body force vector, $\mathbf{b}$, and the element thickness, t, and fluid density, ρ, exact integration yields $\bar{\mathbf{F}}_f^e$ comprised of 2×1 blocks and the 2×1 vector $\bar{\mathbf{F}}_b^e$

$$(\bar{\mathbf{F}}_f^e)_i = \int_{V^e} N_i\mathbf{b}dV = \frac{\rho tJ}{6}\mathbf{b}, \qquad \bar{\mathbf{F}}_b^e = \int_{V^e} N_b\mathbf{b}dV = \frac{9\rho tJ}{40}\mathbf{b} \tag{16}$$

where the subscript i is from 1 to 3. The form of the fluid viscous matrix $\mathbf{K}_f^e$ is similar to that for the stiffness matrix of a solid element in the structure

$$(\mathbf{K}_f^e)_{ij} = \int_{V^e} \mathbf{B}_i^T\mathbf{D}\mathbf{B}_j dV = \frac{tJ}{2}\mathbf{B}_i^T\mathbf{D}\mathbf{B}_j \tag{17}$$

where $\mathbf{D} = \text{diag}(2\mu, 2\mu, \mu)$ = constitutive matrix; and $\mathbf{B}_i$ = strain-velocity matrix defined by spatial derivatives of the shape functions

$$\mathbf{B}_i = \begin{bmatrix} \frac{\partial N_i}{\partial x} & 0 \\ 0 & \frac{\partial N_i}{\partial y} \\ \frac{\partial N_i}{\partial y} & \frac{\partial N_i}{\partial x} \end{bmatrix} \tag{18}$$

The derivatives $\partial N_i/\partial x$ and $\partial N_i/\partial y$ are calculated from the element geometry

$$\frac{\partial N_1}{\partial x} = \frac{y_2 - y_3}{J}, \qquad \frac{\partial N_2}{\partial x} = \frac{y_3 - y_1}{J}, \qquad \frac{\partial N_3}{\partial x} = \frac{y_1 - y_2}{J} \tag{19}$$

and

$$\frac{\partial N_1}{\partial y} = \frac{x_3 - x_2}{J}, \qquad \frac{\partial N_2}{\partial y} = \frac{x_1 - x_3}{J}, \qquad \frac{\partial N_3}{\partial y} = \frac{x_2 - x_1}{J} \tag{20}$$

The fluid viscous matrix defined in Eq. (17) is uncoupled from the viscous matrix for the bubble node (Zienkiewicz et al. 2005), which is defined as

$$\mathbf{K}_b^e = \int_{V^e} \mathbf{B}_b^T\mathbf{D}\mathbf{B}_b dV = \frac{81\mu tJ}{40}\begin{bmatrix} 2\sum\left(\frac{\partial N_i}{\partial x}\right)^2 + \sum\left(\frac{\partial N_i}{\partial y}\right)^2 & \sum\frac{\partial N_i}{\partial x}\frac{\partial N_i}{\partial y} \\ \sum\frac{\partial N_i}{\partial x}\frac{\partial N_i}{\partial y} & \left(\sum\frac{\partial N_i}{\partial x}\right)^2 + 2\left(\sum\frac{\partial N_i}{\partial y}\right)^2 \end{bmatrix} \tag{21}$$

where the definition of $\mathbf{B}_b$ is identical to Eq. (18), but contains derivatives of N_b.

After exact integration, the lumped fluid mass matrices $\mathbf{M}_f^e$ and $\mathbf{M}_b^e$ are uncoupled. Each 2×2 block of $\mathbf{M}_f^e$, the fluid mass matrix for the element corner nodes, is

$$(\mathbf{M}_f^e)_{ii} = \int_{V^e} \rho N_i(N_1 + N_2 + N_3 + N_b)\mathbf{I}_2 dV = \frac{29}{120}\rho tJ\mathbf{I}_2 \tag{22}$$

where $\mathbf{I}_2$ = the 2×2 identity matrix. Similar to the exact integration shown in Eq. (22) for the fluid mass matrix, the 2×2 mass matrix for the bubble node is

$$\mathbf{M}_b^e = \int_{V^e} \rho N_b(N_1 + N_2 + N_3 + N_b)\mathbf{I}_2 dV = \frac{207}{560}\rho tJ\mathbf{I}_2 \tag{23}$$

The gradient operators for corner and bubble nodes are also found by exact integration where each block is

$$(\mathbf{G}_f^e)_{ij} = \int_{V^e} \mathbf{B}_i^T\mathbf{m}N_j dV = \frac{tJ}{6}\mathbf{B}_i^T\mathbf{m},$$
$$(\mathbf{G}_b^e)_j = \int_{V^e} \mathbf{B}_b^T\mathbf{m}N_j dV = -\frac{9}{40}\frac{tJ}{}\mathbf{B}_j^T\mathbf{m} \tag{24}$$

where $\mathbf{G}_f^e$ = 6×3 matrix consisting of 2×1 blocks; $(\mathbf{G}_f^e)_{ij}$ and $\mathbf{m} = [1\,1\,0]^T$ = selection vector; and $\mathbf{G}_b^e$ = 6×1 containing 2×1 blocks $(\mathbf{G}_b^e)_j$.

Numerical Time Integration

For efficient numerical time integration of the fluid response, the nodeless variable, $\mathbf{v}_{f4}^e$ and its time derivative, must be removed from the discrete fluid-element equations [Eqs. (13) and (14)]. To this end, backward Euler time integration is employed, in which case the time derivative of $\mathbf{v}_{f4}^e$ can be expressed as

$$\dot{\mathbf{v}}_{f4}^e = \frac{\mathbf{v}_{f4}^e - \mathbf{v}_{f4_0}^e}{\Delta t} \tag{25}$$

where Δt = simulation time step; and $\mathbf{v}_{f4_0}^e$ = value of $\mathbf{v}_{f4}^e$ at the start of the time step. Assuming the bubble velocity, $\mathbf{v}_b^e$, is equal to the average of the nodal velocities at the start of each time step, $\mathbf{v}_{f4_0}^e$ will be zero according to Eq. (10). This makes $\dot{\mathbf{v}}_{f4}^e = \mathbf{v}_{f4}^e/\Delta t$, which is substituted in to Eq. (13), giving the nodeless velocity

$$\mathbf{v}_{f4}^e = \Delta t(\mathbf{M}_b^e)^{-1}(\mathbf{G}_b^e\mathbf{p}^e + \mathbf{F}_b^e) \tag{26}$$

This result is inserted into Eq. (14) giving

$$\mathbf{G}_f^{eT}\mathbf{v}_f^e + \mathbf{S}^e\mathbf{p}^e = \mathbf{F}_p^e \tag{27}$$

where, $\mathbf{S}^e$ = stabilization matrix

$$\mathbf{S}^e = \mathbf{G}_b^{eT}\left(\frac{\mathbf{M}_b^e}{\Delta t}\right)^{-1}\mathbf{G}_b^e \tag{28}$$

and $\mathbf{F}_p^e$ = right-hand side vector

$$\mathbf{F}_p^e = -\mathbf{G}_b^{eT}\left(\frac{\mathbf{M}_b^e}{\Delta t}\right)^{-1}\mathbf{F}_b^e \tag{29}$$

After assembly of the element response defined in Eqs. (12) and (27), the discrete fluid equations at the global level are

$$\mathbf{M}_f\dot{\mathbf{v}}_f - \mathbf{G}_f\mathbf{p} = \mathbf{F}_f \tag{30}$$

$$\mathbf{G}_f^T\mathbf{v}_f + \mathbf{S}\mathbf{p} = \mathbf{F}_p \tag{31}$$

The equations, along with the structural response equations and the equations that govern the interface response between the structure and fluid, will be differentiated according to the DDM for FSI simulations based on the PFEM.

Discrete Structural Equations

Through the same finite-element procedures, the assembled algebraic equations for the structural response considering material and geometric nonlinear response of the resisting forces are

$$\mathbf{M}_s\dot{\mathbf{v}}_s + \mathbf{C}_s\mathbf{v}_s + \mathbf{F}_s^{\text{int}}(\mathbf{u}_s) = \mathbf{F}_s \tag{32}$$

where $\mathbf{v}_s$ = velocity vector of the structural nodes; $\mathbf{F}_s$ = external load vector; static resisting force vector $\mathbf{F}_s^{\text{int}}$ = nonlinear function of the nodal displacements, $\mathbf{u}_s$, which are related to the velocities through the selected time integration method; and $\mathbf{M}_s$ and $\mathbf{C}_s$ = structural mass and damping matrices, respectively.

Discrete Combined Equations

Particles connected to both the fluid and structural domains are identified as interface particles, whose contributions appear in both fluid and structural equations. From the structural system, the interface equations are extracted from Eq. (32) and assigned additional i and s subscripts

$$\mathbf{M}_{ss}\dot{\mathbf{v}}_s + \mathbf{M}_{si}\dot{\mathbf{v}}_i + \mathbf{C}_{ss}\mathbf{v}_s + \mathbf{C}_{si}\mathbf{v}_i + \mathbf{F}_s^{\text{int}}(\mathbf{u}_s, \mathbf{u}_i) = \mathbf{F}_s \tag{33}$$

$$\mathbf{M}_{is}\dot{\mathbf{v}}_s + \mathbf{M}_{ii}^s\dot{\mathbf{v}}_i + \mathbf{C}_{is}\mathbf{v}_s + \mathbf{C}_{ii}\mathbf{v}_i + \mathbf{F}_i^{\text{int}}(\mathbf{u}_s, \mathbf{u}_i) = \mathbf{F}_i^s \tag{34}$$

where $\mathbf{v}_i$ = velocity vector of the interface particles. Similarly, the interface equations are extracted from Eqs. (30) and (31) for the fluid domain and given additional i and f subscripts

$$\mathbf{M}_{ff}\dot{\mathbf{v}}_f - \mathbf{G}_f\mathbf{p} = \mathbf{F}_f \tag{35}$$

$$\mathbf{M}_{ii}^f\dot{\mathbf{v}}_i - \mathbf{G}_i\mathbf{p} = \mathbf{F}_i^f \tag{36}$$

$$\mathbf{G}_f^T\mathbf{v}_f + \mathbf{G}_i^T\mathbf{v}_i + \mathbf{S}\mathbf{p} = \mathbf{F}_p \tag{37}$$

Eqs. (34) and (36) are combined in order to solve for the particle response on the fluid–structure interface

$$\mathbf{M}_{is}\dot{\mathbf{v}}_s + (\mathbf{M}_{ii}^s + \mathbf{M}_{ii}^f)\dot{\mathbf{v}}_i + \mathbf{C}_{is}\mathbf{v}_s + \mathbf{C}_{ii}\mathbf{v}_i + \mathbf{F}_i^{\text{int}}(\mathbf{u}_s, \mathbf{u}_i) - \mathbf{G}_i\mathbf{p} = \mathbf{F}_i^s + \mathbf{F}_i^f \tag{38}$$

Eqs. (33), (35), (37), and (38) are the combined equations for FSI response analysis by the PFEM. Their solution via numerical time approximation is briefly summarized next.

Time Integration of FSI Response

The solution of Eqs. (33), (35), (37), and (38) requires a set of primary unknowns and numerical approximations relating these unknowns to other quantities. Choosing particle velocity and pressure as primary unknowns, the backward Euler method relates the acceleration to velocity according to

$$\dot{\mathbf{v}}_n = \frac{\mathbf{v}_n - \mathbf{v}_{n-1}}{\Delta t} \tag{39}$$

where the subscript n = response at the current time step and $n-1$ at the previous time step. Similarly, the relationship between displacement and velocity is

$$\mathbf{u}_n = \mathbf{u}_{n-1} + \Delta t\mathbf{v}_n \tag{40}$$

These approximations are applied to all fluid, structure, and interface particles.

Fixed-point iteration can be applied to the combined equations in order to obtain a monolithic system of equations, which is solved by the fractional step method (FSM). The resulting time-discretized equations in residual form for response of the fluid domain are then

$$\frac{\mathbf{M}_{ff,n}}{\Delta t}\Delta\mathbf{v}_{f,n} - \mathbf{G}_{f,n}\Delta\mathbf{p}_n = \mathbf{r}_{f,n} \tag{41}$$

$$\mathbf{G}_{f,n}^T\Delta\mathbf{v}_{f,n} + \mathbf{G}_{i,n}^T\Delta\mathbf{v}_{i,n} + \mathbf{S}_n\Delta\mathbf{p}_n = \mathbf{r}_{p,n} \tag{42}$$

and those for the structural domain are

$$\left(\frac{\mathbf{M}_{ss,n}}{\Delta t} + \mathbf{C}_{ss,n} + \Delta t\mathbf{K}_{ss,n}\right)\Delta\mathbf{v}_{s,n} + \left(\frac{\mathbf{M}_{si,n}}{\Delta t} + \mathbf{C}_{si,n} + \Delta t\mathbf{K}_{si,n}\right)\Delta\mathbf{v}_{i,n} = \mathbf{r}_{s,n} \tag{43}$$

For the response of the interface, the equations are

$$\left(\frac{\mathbf{M}_{is,n}}{\Delta t}+\mathbf{C}_{is,n}+\Delta t\mathbf{K}_{is,n}\right)\Delta\mathbf{v}_{s,n}+\left[\frac{(\mathbf{M}^{s}_{ii,n}+\mathbf{M}^{f}_{ii,n})}{\Delta t}+\mathbf{C}_{ii,n}+\Delta t\mathbf{K}_{ii,n}\right]\Delta\mathbf{v}_{i,n}-\mathbf{G}_{i,n}\mathbf{p}_{n}=\mathbf{r}_{i,n} \tag{44}$$

where, $\mathbf{r}_f$, $\mathbf{r}_p$, $\mathbf{r}_s$, and $\mathbf{r}_i$ = residual vectors of each equation; and $\mathbf{K}_{ss,n}$, $\mathbf{K}_{si,n}$, $\mathbf{K}_{is,n}$, and $\mathbf{K}_{ii,n}$ = tangents of resisting force vector to unknowns as defined as

$$\mathbf{K}_{ss,n}=\frac{\partial\mathbf{F}^{\text{int}}_{s,n}}{\partial\mathbf{u}_s},\qquad \mathbf{K}_{si,n}=\frac{\partial\mathbf{F}^{\text{int}}_{s,n}}{\partial\mathbf{u}_i},\qquad \mathbf{K}_{is,n}=\frac{\partial\mathbf{F}^{\text{int}}_{i,n}}{\partial\mathbf{u}_s},\qquad \mathbf{K}_{ii,n}=\frac{\partial\mathbf{F}^{\text{int}}_{i,n}}{\partial\mathbf{u}_i} \tag{45}$$

Further details on the residual functions, governing equations, and their solution by the FSM can be found in Zhu and Scott (2014a) but are omitted herein given that sufficient details have been shown for their subsequent differentiation according to the DDM.

Direct Differentiation of the PFEM

The application of the DDM to FSI simulations based on the PFEM requires differentiation of the discrete equations that govern the fluid and structural response. However, for large displacement applications such as FSI, additional terms that arise from updating the configuration at each iteration must be taken in to account in the derivation of sensitivity equations. The direct differentiation method (DDM) is used here to compute the sensitivity of PFEM analysis with FSM. As in Kleiber et al. (1997), the DDM is applied on the fluid Eqs. (30) and (31), and structural Eq. (32) to develop the sensitivity equations for fluid and structure. Then the combined sensitivity equations for FSI are obtained taking in to account both material and geometric nonlinearity.

Fluid Sensitivity Equations

Taking the derivative of the discrete fluid equations [Eqs. (30) and (31)] with respect to an uncertain parameter, θ, gives

$$\mathbf{M}_f\frac{\partial\dot{\mathbf{v}}_f}{\partial\theta}-\mathbf{G}_f\frac{\partial\mathbf{p}}{\partial\theta}+\mathbf{H}\frac{\partial\mathbf{u}_f}{\partial\theta}=\left.\frac{\partial\mathbf{F}_f}{\partial\theta}\right|_{\mathbf{u}_f}-\left.\frac{\partial\mathbf{M}_f}{\partial\theta}\right|_{\mathbf{u}_f}\dot{\mathbf{v}}_f+\left.\frac{\partial\mathbf{G}_f}{\partial\theta}\right|_{\mathbf{u}_f}\mathbf{p} \tag{46}$$

$$\mathbf{G}_f^T\frac{\partial\mathbf{v}_f}{\partial\theta}+\mathbf{S}\frac{\partial\mathbf{p}}{\partial\theta}+\mathbf{T}\frac{\partial\mathbf{u}_f}{\partial\theta}=\left.\frac{\partial\mathbf{F}_p}{\partial\theta}\right|_{\mathbf{u}_f}-\left.\frac{\partial\mathbf{G}_f^T}{\partial\theta}\right|_{\mathbf{u}_f}\mathbf{v}_f-\left.\frac{\partial\mathbf{S}}{\partial\theta}\right|_{\mathbf{u}_f}\mathbf{p} \tag{47}$$

where $\partial\mathbf{u}_f/\partial\theta$, $\partial\mathbf{v}_f/\partial\theta$, $\partial\dot{\mathbf{v}}_f/\partial\theta$, and $\partial\mathbf{p}/\partial\theta$ = sensitivity of fluid displacements, velocities, accelerations, and pressures, respectively. On the right-hand side, all derivatives with respect to θ are taken with fluid displacements $\mathbf{u}_f$ fixed. On the left-hand side, the matrices $\mathbf{H}$ and $\mathbf{T}$ are partial derivatives that account for geometric nonlinearity of the fluid response

$$\mathbf{H}=\frac{\partial(\mathbf{M}_f\dot{\mathbf{v}}_f)}{\partial\mathbf{u}_f}-\frac{\partial(\mathbf{G}_f\mathbf{p})}{\partial\mathbf{u}_f}-\frac{\partial\mathbf{F}_f}{\partial\mathbf{u}_f} \tag{48}$$

$$\mathbf{T}=\frac{\partial(\mathbf{G}_f^T\mathbf{v}_f)}{\partial\mathbf{u}_f}+\frac{\partial(\mathbf{S}\mathbf{p})}{\partial\mathbf{u}_f}-\frac{\partial\mathbf{F}_p}{\partial\mathbf{u}_f} \tag{49}$$

These terms affect the fluid response sensitivity but do not depend on the uncertain parameter, θ. The matrices shown in Eqs. (48) and (49) are assembled from the derivatives of the element contributions defined in Eqs. (16)–(24) with respect to element displacements. For instance, the kth column of the derivative of the element inertial forces from Eq. (48) is defined as

$$\left(\frac{\partial(\mathbf{M}^e_f\dot{\mathbf{v}}^e_f)}{\partial\mathbf{u}^e_f}\right)_k=\frac{\partial\mathbf{M}^e_f}{\partial u^e_{fk}}\dot{\mathbf{v}}^e_f,\qquad \left(\frac{\partial\mathbf{M}^e_f}{\partial u^e_{fk}}\right)_{ii}=\frac{29\rho t}{120}\frac{\partial J}{\partial u^e_{fk}}\mathbf{I}_2 \tag{50}$$

where $\mathbf{M}^e_f$ was defined in Eq. (22) and the element acceleration vector, $\dot{\mathbf{v}}^e_f$, is known at the end of the simulation time step. As shown in Eq. (7), the Jacobian, J, is a function of the element displacements. The derivatives of J with respect to the horizontal and vertical displacements of node 1 are

$$\frac{\partial J}{\partial u^e_{f1}}=y_2-y_3,\qquad \frac{\partial J}{\partial u^e_{f2}}=x_3-x_2 \tag{51}$$

where the derivatives with respect to other nodal displacements can be calculated similarly.

The kth column of the geometric tangent matrix for the gradient operator is defined as

$$\left[\frac{\partial(\mathbf{G}^e_f\mathbf{p}^e)}{\partial\mathbf{u}^e_f}\right]_k=\frac{\partial\mathbf{G}^e_f}{\partial u^e_{fk}}\mathbf{p}^e,\qquad \left(\frac{\partial\mathbf{G}^e_f}{\partial u^e_{fk}}\right)_{ij}=\frac{t}{6}\left(\frac{\partial J}{\partial u^e_{fk}}\mathbf{B}_i^T\mathbf{m}+J\frac{\partial\mathbf{B}_i^T}{\partial u^e_{fk}}\mathbf{m}\right) \tag{52}$$

where $\mathbf{G}^e_f$ was defined in Eq. (24) and the pressure $\mathbf{p}^e$ is known at the end of the simulation time step when the response sensitivity is computed. The derivative of the strain-velocity matrix, $\mathbf{B}_i$ defined in Eq. (18), with respect to nodal displacements is

$$\frac{\partial\mathbf{B}_1}{\partial u^e_{f1}}=-\frac{1}{J^2}\begin{bmatrix}(y_2-y_3)^2 & 0\\ 0 & (x_3-x_2)^2\\ (x_3-x_2)^2 & (y_2-y_3)^2\end{bmatrix} \tag{53}$$

Derivatives with respect to other nodal displacements for $\mathbf{B}_1$, $\mathbf{B}_2$, and $\mathbf{B}_3$ have similar definitions.

For the right-hand side vector, $\mathbf{F}^e_f$, defined in Eq. (15), the kth column of the geometric tangent matrix is

$$\left(\frac{\partial\mathbf{F}^e_f}{\partial\mathbf{u}^e_f}\right)_k=\left(\frac{\partial\bar{\mathbf{F}}^e_f}{\partial\mathbf{u}^e_f}\right)_k-\left(\frac{\partial\mathbf{K}^e_f\mathbf{v}^e_f}{\partial\mathbf{u}^e_f}\right)_k=\frac{\partial\bar{\mathbf{F}}^e_f}{\partial u^e_{fk}}-\frac{\partial\mathbf{K}^e_f}{\partial u^e_{fk}}\mathbf{v}^e_f \tag{54}$$

As defined in Eqs. (16) and (17), derivatives of $\bar{\mathbf{F}}^e_f$ and $\mathbf{K}^e_f$ are taken with respect to displacements

$$\left(\frac{\partial\bar{\mathbf{F}}^e_f}{\partial u^e_{fk}}\right)_i=\frac{\rho t}{6}\frac{\partial J}{\partial u^e_{fk}}\mathbf{b},\qquad \left(\frac{\partial\mathbf{K}^e_f}{\partial u^e_{fk}}\right)_{ij}=\frac{t}{2}\left(\frac{\partial J}{\partial u^e_{fk}}\mathbf{B}_i^T\mathbf{D}\mathbf{B}_j+J\frac{\partial\mathbf{B}_i^T}{\partial u^e_{fk}}\mathbf{D}\mathbf{B}_j+J\mathbf{B}_i\mathbf{D}\frac{\partial\mathbf{B}_j^T}{\partial u^e_{fk}}\right) \tag{55}$$

In the same manner, the kth column of the geometric tangent matrices for the stabilization matrix $\mathbf{S}^e$ and vector $\mathbf{F}^e_p$ are defined as

$$\left(\frac{\partial(\mathbf{S}^e\mathbf{p}^e)}{\partial \mathbf{u}_f^e}\right)_k = \frac{\partial \mathbf{S}^e}{\partial u_{fk}^e}\mathbf{p}^e, \qquad \left(\frac{\partial \mathbf{F}_p^e}{\partial \mathbf{u}_f^e}\right)_k = \frac{\partial \mathbf{F}_p^e}{\partial u_{fk}^e} \tag{56}$$

where the original expressions of $\mathbf{S}^e$ and $\mathbf{F}_p^e$ defined in Eqs. (28) and (29), are triple multiplication of matrices and vectors including a matrix inverse, leading to several terms for their derivatives

$$\frac{\partial \mathbf{S}^e}{\partial u_{fk}^e} = \frac{\partial \mathbf{G}_b^{eT}}{\partial u_{fk}^e}\left(\frac{\mathbf{M}_b^e}{\Delta t}\right)^{-1}\mathbf{G}_b^e + \mathbf{G}_b^{eT}\frac{\partial\left(\frac{\mathbf{M}_b^e}{\Delta t}\right)^{-1}}{\partial u_{fk}^e}\mathbf{G}_b^e + \mathbf{G}_b^{eT}\left(\frac{\mathbf{M}_b^e}{\Delta t}\right)^{-1}\frac{\partial \mathbf{G}_b^e}{\partial u_{fk}^e} \tag{57}$$

$$\frac{\partial \mathbf{F}_p^e}{\partial u_{fk}^e} = -\frac{\partial \mathbf{G}_b^{eT}}{\partial u_{fk}^e}\left(\frac{\mathbf{M}_b^e}{\Delta t}\right)^{-1}\mathbf{F}_b^e - \mathbf{G}_b^{eT}\frac{\partial\left(\frac{\mathbf{M}_b^e}{\Delta t}\right)^{-1}}{\partial u_{fk}^e}\mathbf{F}_b^e - \mathbf{G}_b^{eT}\left(\frac{\mathbf{M}_b^e}{\Delta t}\right)^{-1}\frac{\partial \mathbf{F}_b^e}{\partial u_{fk}^e} \tag{58}$$

where $\mathbf{M}_b^e$, $\mathbf{G}_b^e$, and $\mathbf{F}_b^e$ are defined in Eqs. (23), (24), and (15), respectively. The derivative of the mass matrix for the bubble node is

$$\frac{\partial(\mathbf{M}_b^{e-1})}{\partial u_{fk}^e} = -\frac{560}{207\rho t J^2}\frac{\partial J}{\partial u_{fk}^e}\mathbf{I}_2 \tag{59}$$

while the derivative of the gradient operator for the bubble node is

$$\left(\frac{\partial \mathbf{G}_b^e}{\partial u_{fk}^e}\right)_j = -\frac{9}{40}\frac{t}{}\left(\frac{\partial J}{\partial u_{fk}^e}\mathbf{B}_j^T\mathbf{m} + J\frac{\partial \mathbf{B}_j^T}{\partial u_{fk}^e}\mathbf{m}\right) \tag{60}$$

The derivative of the right-hand side vector, $\mathbf{F}_b^e$, defined in Eq. (16), is also similar to that shown in Eqs. (54) and (55)

$$\frac{\partial \mathbf{F}_b^e}{\partial u_{fk}^e} = \frac{\partial \bar{\mathbf{F}}_b^e}{\partial u_{fk}^e} - \frac{\partial \mathbf{K}_b^e}{\partial u_{fk}^e}\mathbf{v}_b^e \tag{61}$$

where the derivative of the force vector is

$$\frac{\partial \bar{\mathbf{F}}_b^e}{\partial u_{fk}^e} = \frac{9\rho t}{40}\frac{\partial J}{\partial u_{fk}^e}\mathbf{b} \tag{62}$$

The derivative of the viscosity matrix for the bubble node [defined in Eq. (21)] becomes complex due to the nonlinearity of the shape function, N_b, defined in Eq. (11), for the bubble DOFs

$$\frac{\partial \mathbf{K}_b^e}{\partial u_{fk}^e} = \frac{81\mu t}{40}\left\{\frac{\partial J}{\partial u_{fk}^e}\begin{bmatrix} 2\sum\left(\frac{\partial N_i}{\partial x}\right)^2 + \sum\left(\frac{\partial N_i}{\partial y}\right)^2 & \sum\frac{\partial N_i}{\partial x}\frac{\partial N_i}{\partial y} \\ \sum\frac{\partial N_i}{\partial x}\frac{\partial N_i}{\partial y} & \left(\sum\frac{\partial N_i}{\partial x}\right)^2 + 2\left(\sum\frac{\partial N_i}{\partial y}\right)^2 \end{bmatrix} + J\begin{bmatrix} 4\sum\left(\frac{\partial^2 N_i}{\partial x\partial u_{fk}^e}\right) + 2\sum\left(\frac{\partial^2 N_i}{\partial y\partial u_{fk}^e}\right) & \sum\frac{\partial^2 N_i}{\partial x\partial u_{fk}^e}\frac{\partial N_i}{\partial y} + \sum\frac{\partial N_i}{\partial x}\frac{\partial^2 N_i}{\partial y\partial u_{fk}^e} \\ \sum\frac{\partial^2 N_i}{\partial x\partial u_{fk}^e}\frac{\partial N_i}{\partial y} + \sum\frac{\partial N_i}{\partial x}\frac{\partial^2 N_i}{\partial y\partial u_{fk}^e} & 2\sum\left(\frac{\partial^2 N_i}{\partial x\partial u_{fk}^e}\right) + 4\sum\left(\frac{\partial^2 N_i}{\partial y\partial u_{fk}^e}\right) \end{bmatrix}\right\} \tag{63}$$

As shown in Eq. (8), the displacements u_{fk}^e differ with x and y only by a constant. Therefore, the derivatives $\partial/\partial u_{fk}^e$ are equivalent to $\partial/\partial x$ or $\partial/\partial y$ and are easily computed.

Structural Sensitivity Equations

The DDM is also applied to the nonlinear structural response in Eq. (32)

$$\mathbf{M}_s\frac{\partial \dot{\mathbf{v}}_s}{\partial\theta} + \mathbf{C}_s\frac{\partial \mathbf{v}_s}{\partial\theta} + \mathbf{K}_s\frac{\partial \mathbf{u}_s}{\partial\theta} = \frac{\partial \mathbf{F}_s}{\partial\theta} - \left.\frac{\partial \mathbf{M}_s}{\partial\theta}\right|_{\mathbf{u}_s}\dot{\mathbf{v}}_s - \left.\frac{\partial \mathbf{C}_s}{\partial\theta}\right|_{\mathbf{u}_s}\mathbf{v}_s - \left.\frac{\partial \mathbf{F}_s^{\text{int}}}{\partial\theta}\right|_{\mathbf{u}_s} \tag{64}$$

where $\partial\mathbf{u}_s/\partial\theta$, $\partial\mathbf{v}_s/\partial\theta$, and $\partial\dot{\mathbf{v}}_s/\partial\theta$ = sensitivity of structural displacements, velocities, and accelerations. All the derivatives on the right-hand side are partial derivatives with structural displacements $\mathbf{u}_s$ fixed. On the left-hand side, $\mathbf{K}_s$ is the tangent stiffness matrix, or the derivative of the static resisting forces with respect to nodal displacements of $\mathbf{F}_s^{\text{int}}$ as defined in Eq. (45). Additional details on the implementation of the DDM for finite-element simulations of nonlinear structural dynamics can be found in Franchin (2004).

Combined Sensitivity Equations

Following the same strategy as for Eqs. (33) and (34), the interface equations for structural sensitivity are extracted from Eq. (64) and assigned additional i and s subscripts,

$$\mathbf{M}_{ss}\frac{\partial \dot{\mathbf{v}}_s}{\partial\theta} + \mathbf{M}_{si}\frac{\partial \dot{\mathbf{v}}_i}{\partial\theta} + \mathbf{C}_{ss}\frac{\partial \mathbf{v}_s}{\partial\theta} + \mathbf{C}_{si}\frac{\partial \mathbf{v}_i}{\partial\theta} + \mathbf{K}_{ss}\frac{\partial \mathbf{u}_s}{\partial\theta} + \mathbf{K}_{si}\frac{\partial \mathbf{u}_i}{\partial\theta} = \frac{\partial \mathbf{F}_s}{\partial\theta} - \frac{\partial \mathbf{M}_{ss}}{\partial\theta}\dot{\mathbf{v}}_s - \frac{\partial \mathbf{M}_{si}}{\partial\theta}\dot{\mathbf{v}}_i - \frac{\partial \mathbf{C}_{ss}}{\partial\theta}\mathbf{v}_s - \frac{\partial \mathbf{C}_{si}}{\partial\theta}\mathbf{v}_i - \frac{\partial \mathbf{F}_s^{\text{int}}}{\partial\theta} \tag{65}$$

$$\mathbf{M}_{is}\frac{\partial \dot{\mathbf{v}}_s}{\partial\theta} + \mathbf{M}_{ii}^s\frac{\partial \dot{\mathbf{v}}_i}{\partial\theta} + \mathbf{C}_{is}\frac{\partial \mathbf{v}_s}{\partial\theta} + \mathbf{C}_{ii}\frac{\partial \mathbf{v}_i}{\partial\theta} + \mathbf{K}_{is}\frac{\partial \mathbf{u}_s}{\partial\theta} + \mathbf{K}_{ii}\frac{\partial \mathbf{u}_i}{\partial\theta} = \frac{\partial \mathbf{F}_i^s}{\partial\theta} - \frac{\partial \mathbf{M}_{is}}{\partial\theta}\dot{\mathbf{v}}_s - \frac{\partial \mathbf{M}_{ii}^s}{\partial\theta}\dot{\mathbf{v}}_i - \frac{\partial \mathbf{C}_{is}}{\partial\theta}\mathbf{v}_s - \frac{\partial \mathbf{C}_{ii}}{\partial\theta}\mathbf{v}_i - \frac{\partial \mathbf{F}_i^{\text{int}}}{\partial\theta} \tag{66}$$

Similarly, the fluid sensitivity from Eqs. (46) and (47) are also split and given additional i and f subscripts

$$\mathbf{M}_{ff}\frac{\partial \dot{\mathbf{v}}_f}{\partial\theta} - \mathbf{G}_f\frac{\partial \mathbf{p}}{\partial\theta} + \mathbf{H}_{ff}\frac{\partial \mathbf{u}_f}{\partial\theta} + \mathbf{H}_{fi}\frac{\partial \mathbf{u}_i}{\partial\theta} = \frac{\partial \mathbf{F}_f}{\partial\theta} - \frac{\partial \mathbf{M}_{ff}}{\partial\theta}\dot{\mathbf{v}}_f + \frac{\partial \mathbf{G}_f}{\partial\theta}\mathbf{p} \tag{67}$$

$$\mathbf{M}_{ii}^f\frac{\partial \dot{\mathbf{v}}_i}{\partial\theta} - \mathbf{G}_i\frac{\partial \mathbf{p}}{\partial\theta} + \mathbf{H}_{\text{if}}\frac{\partial \mathbf{u}_f}{\partial\theta} + \mathbf{H}_{ii}\frac{\partial \mathbf{u}_i}{\partial\theta} = \frac{\partial \mathbf{F}_i^f}{\partial\theta} - \frac{\partial \mathbf{M}_{ii}^f}{\partial\theta}\dot{\mathbf{v}}_i + \frac{\partial \mathbf{G}_i}{\partial\theta}\mathbf{p} \tag{68}$$

$$\mathbf{G}_f^T\frac{\partial \mathbf{v}_f}{\partial\theta} + \mathbf{G}_i^T\frac{\partial \mathbf{v}_i}{\partial\theta} + \mathbf{S}\frac{\partial \mathbf{p}}{\partial\theta} + \mathbf{T}_f\frac{\partial \mathbf{u}_f}{\partial\theta} + \mathbf{T}_i\frac{\partial \mathbf{u}_i}{\partial\theta} = \frac{\partial \mathbf{F}_p}{\partial\theta} - \frac{\partial \mathbf{G}_f^T}{\partial\theta}\mathbf{v}_f - \frac{\partial \mathbf{G}_i^T}{\partial\theta}\mathbf{v}_i - \frac{\partial \mathbf{S}}{\partial\theta}\mathbf{p} \tag{69}$$

The sensitivity equations for the interface are a combination of Eqs. (66) and (68)

$$\mathbf{M}_{is}\frac{\partial \dot{\mathbf{v}}_s}{\partial \theta}+(\mathbf{M}_{ii}^s+\mathbf{M}_{ii}^f)\frac{\partial \dot{\mathbf{v}}_i}{\partial \theta}+\mathbf{C}_{is}\frac{\partial \mathbf{v}_s}{\partial \theta}+\mathbf{C}_{ii}\frac{\partial \mathbf{v}_i}{\partial \theta}+\mathbf{K}_{is}\frac{\partial \mathbf{u}_s}{\partial \theta}+(\mathbf{K}_{ii}+\mathbf{H}_{ii})\frac{\partial \mathbf{u}_i}{\partial \theta}+\mathbf{H}_{\text{if}}\frac{\partial \mathbf{u}_f}{\partial \theta}-\mathbf{G}_i\frac{\partial \mathbf{p}}{\partial \theta}=\frac{\partial \mathbf{F}_i^s}{\partial \theta}+\frac{\partial \mathbf{F}_i^f}{\partial \theta}-\frac{\partial \mathbf{M}_{is}}{\partial \theta}\dot{\mathbf{v}}_s-\left(\frac{\partial \mathbf{M}_{ii}^s}{\partial \theta}+\frac{\partial \mathbf{M}_{ii}^f}{\partial \theta}\right)\dot{\mathbf{v}}_i-\frac{\partial \mathbf{C}_{is}}{\partial \theta}\mathbf{v}_s-\frac{\partial \mathbf{C}_{ii}}{\partial \theta}\mathbf{v}_i-\frac{\partial \mathbf{F}_i^{\text{int}}}{\partial \theta}+\frac{\partial \mathbf{G}_i}{\partial \theta}\mathbf{p} \tag{70}$$

Eqs. (65), (67), (69), and (70) represent the combined equations for sensitivity analysis of FSI via the PFEM.

Numerical Solution of DDM Equations

The foregoing combined equations for DDM sensitivity analysis of the PFEM are continuous in time, save for the numerical approximation at the element level for the bubble node. Consistent differentiation of the time-discretized equations is necessary for proper implementation of the DDM (Conte et al. 2003). Using backward Euler time integration at the global level, it is straightforward to express the derivatives of acceleration and displacement in terms of the primary unknown velocity

$$\frac{\partial \dot{\mathbf{v}}_n}{\partial \theta}=\frac{1}{\Delta t}\left(\frac{\partial \mathbf{v}_n}{\partial \theta}-\frac{\partial \mathbf{v}_{n-1}}{\partial \theta}\right) \tag{71}$$

with identical expressions for the acceleration sensitivity of fluid and interface particles. Similarly, the relationship between the derivatives of displacement and velocity for backward Euler time integration is

$$\frac{\partial \mathbf{u}_n}{\partial \theta}=\frac{\partial \mathbf{u}_{n-1}}{\partial \theta}+\Delta t\frac{\partial \mathbf{v}_n}{\partial \theta} \tag{72}$$

again with identical expressions of the displacement sensitivity of fluid and interface particles. With these numerical approximations, the solution for the response sensitivity follows the same process as that required for the PFEM response (Zhu and Scott 2014a), save for the geometric nonlinearity terms, $\mathbf{H}$ and $\mathbf{T}$. Retaining these terms on the left-hand side when solving for the sensitivity according to Eqs. (67), (69), and (70) would make the solution for the sensitivity inconsistent with that used for the PFEM response via the FSM. To avoid this inconsistency, the geometric nonlinearity terms are moved to the right-hand side with values of particle velocity sensitivity from the previous time step. The resulting time-discretized equations for sensitivity of the fluid domain are then

$$\frac{\mathbf{M}_{ff,n}}{\Delta t}\frac{\partial \mathbf{v}_{f,n}}{\partial \theta}-\mathbf{G}_{f,n}\frac{\partial \mathbf{p}_n}{\partial \theta}=\frac{\partial \mathbf{F}_{f,n}}{\partial \theta}+\frac{\mathbf{M}_{ff,n}}{\Delta t}\frac{\partial \mathbf{v}_{f,n-1}}{\partial \theta}-\frac{\partial \mathbf{M}_{ff,n}}{\partial \theta}\dot{\mathbf{v}}_{f,n}+\frac{\partial \mathbf{G}_{f,n}}{\partial \theta}\mathbf{p}_n-\mathbf{H}_{ff,n}\frac{\partial \mathbf{u}_{f,n-1}}{\partial \theta}-\mathbf{H}_{fi,n}\frac{\partial \mathbf{u}_{i,n-1}}{\partial \theta} \tag{73}$$

$$\mathbf{G}_{f,n}^T\frac{\partial \mathbf{v}_{f,n}}{\partial \theta}+\mathbf{G}_{i,n}^T\frac{\partial \mathbf{v}_{i,n}}{\partial \theta}+\mathbf{S}_n\frac{\partial \mathbf{p}_n}{\partial \theta}=\frac{\partial \mathbf{F}_{p,n}}{\partial \theta}-\frac{\partial \mathbf{G}_{f,n}^T}{\partial \theta}\mathbf{v}_{f,n}-\frac{\partial \mathbf{G}_{i,n}^T}{\partial \theta}\mathbf{v}_{i,n}-\frac{\partial \mathbf{S}_n}{\partial \theta}\mathbf{p}_n-\mathbf{T}_{f,n}\frac{\partial \mathbf{u}_{f,n-1}}{\partial \theta}-\mathbf{T}_{i,n}\frac{\partial \mathbf{u}_{i,n-1}}{\partial \theta} \tag{74}$$

while those for the structural domain are

$$\left(\frac{\mathbf{M}_{ss,n}}{\Delta t}+\mathbf{C}_{ss,n}+\Delta t\mathbf{K}_{ss,n}\right)\frac{\partial \mathbf{v}_{s,n}}{\partial \theta}+\left(\frac{\mathbf{M}_{si,n}}{\Delta t}+\mathbf{C}_{si,n}+\Delta t\mathbf{K}_{si,n}\right)\frac{\partial \mathbf{v}_{i,n}}{\partial \theta}=\frac{\partial \mathbf{F}_{s,n}}{\partial \theta}+\frac{\mathbf{M}_{ss,n}}{\Delta t}\frac{\partial \mathbf{v}_{s,n-1}}{\partial \theta}+\frac{\mathbf{M}_{ss,n}}{\Delta t}\frac{\partial \mathbf{v}_{s,n-1}}{\partial \theta}-\left.\frac{\partial \mathbf{M}_{s,n}}{\partial \theta}\right|_{\mathbf{u}_s}\dot{\mathbf{v}}_{s,n}-\left.\frac{\partial \mathbf{C}_{s,n}}{\partial \theta}\right|_{\mathbf{u}_s}\mathbf{v}_{s,n}-\left.\frac{\partial \mathbf{F}_{s,n}^{\text{int}}}{\partial \theta}\right|_{\mathbf{u}_s} \tag{75}$$

The sensitivity of the time discretized equations for the interface response are

$$\left(\frac{\mathbf{M}_{is,n}}{\Delta t}+\mathbf{C}_{is,n}+\Delta t\mathbf{K}_{is,n}\right)\frac{\partial \mathbf{v}_{s,n}}{\partial \theta}+\left(\frac{(\mathbf{M}_{ii,n}^s+\mathbf{M}_{ii,n}^f)}{\Delta t}+\mathbf{C}_{ii,n}+\Delta t\mathbf{K}_{ii,n}\right)\frac{\partial \mathbf{v}_{i,n}}{\partial \theta}-\mathbf{G}_{i,n}\frac{\partial \mathbf{p}_n}{\partial \theta}=\frac{\partial \mathbf{F}_{i,n}^s}{\partial \theta}+\frac{\partial \mathbf{F}_{i,n}^f}{\partial \theta}+\frac{\mathbf{M}_{is,n}}{\Delta t}\frac{\partial \mathbf{v}_{s,n-1}}{\partial \theta}+\frac{(\mathbf{M}_{ii,n}^s+\mathbf{M}_{ii,n}^f)}{\Delta t}\frac{\partial \mathbf{v}_{i,n-1}}{\partial \theta}-\frac{\partial \mathbf{M}_{is,n}}{\partial \theta}\dot{\mathbf{v}}_{s,n}-\left(\frac{\partial \mathbf{M}_{ii,n}^s}{\partial \theta}+\frac{\partial \mathbf{M}_{ii,n}^f}{\partial \theta}\right)\dot{\mathbf{v}}_{i,n}-\frac{\partial \mathbf{C}_{is,n}}{\partial \theta}\mathbf{v}_{s,n}-\frac{\partial \mathbf{C}_{ii,n}}{\partial \theta}\mathbf{v}_{i,n}-\frac{\partial \mathbf{F}_{i,n}^{\text{int}}}{\partial \theta}+\frac{\partial \mathbf{G}_{i,n}}{\partial \theta}\mathbf{p}_n-\mathbf{H}_{ii,n}\frac{\partial \mathbf{u}_{i,n-1}}{\partial \theta}-\mathbf{H}_{\text{if},n}\frac{\partial \mathbf{u}_{f,n-1}}{\partial \theta} \tag{76}$$

For a single parameter, θ, of the FSI model, the right-hand sides of Eqs. (73)–(76) are assembled from element contributions. For the structural frame elements, DDM formulations are available in the literature (Scott et al. 2004; Conte et al. 2004), while contributions of the fluid elements is based on differentiation of the closed form expressions in Eqs. (16)–(24) with respect to θ. For example, the derivative of the fluid mass matrix defined in Eq. (22) is

$$\frac{\partial \mathbf{M}_f^e}{\partial \theta}=\frac{29}{120}\left(\frac{\partial \rho}{\partial \theta}tJ+\rho\frac{\partial t}{\partial \theta}J+\rho t\frac{\partial J}{\partial \theta}\right)\mathbf{I}_2 \tag{77}$$

where $\partial\rho/\partial\theta$ and $\partial t/\partial\theta$ are equal to 0 or 1 depending on which parameter is chosen. The derivative $\partial J/\partial\theta$ corresponds to the geometric sensitivity and is a function of the nodal displacement sensitivity, $\partial u_{fk}^e/\partial\theta$, consistent with differention of Eq. (7) with respect to θ. Similar expressions for the aforementioned fluid matrices and vectors can be calculated. The solution for the derivatives of velocity and pressure are computed using the same FSM solver as the ordinary response in Eqs. (41)–(44) because the left-hand side matrices are the same as those in Eqs. (73)–(76).

This computational process of forming a right-hand side vector and solving for the sensitivity using the same left-hand side system

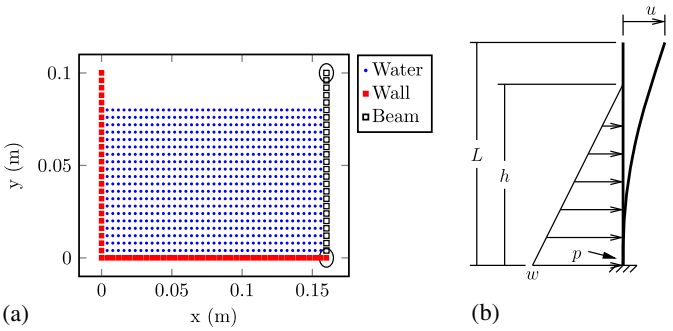

Fig. 2. Model for elastic structure interacting with static water

is repeated for each parameter in the FSI model. The steps have been implemented within the finite-element response sensitivity framework of *OpenSees* (Scott and Haukaas 2008). Further details of the PFEM implementation for computing deterministic FSI response in *OpenSees* are described in Zhu and Scott (2014b).

Examples

In the following examples, the PFEM sensitivity calculated by the DDM is compared to analytical solutions of FSI and to the results of finite-difference calculations for more-complex FSI simulations involving nonlinear structural response.

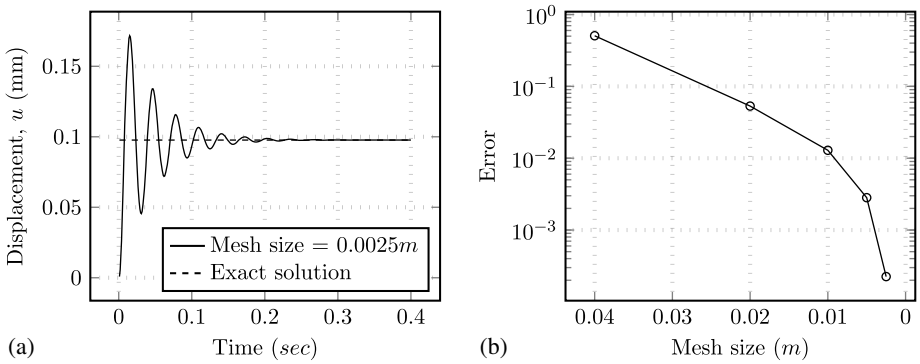

Fig. 3. Displacement of tip node and convergence with respect to mesh size: (a) tip displacement; (b) displacement convergence

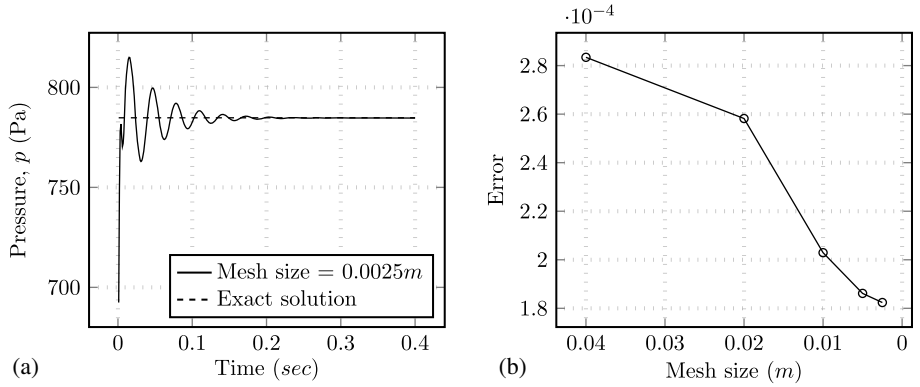

Fig. 4. Pressure of base node and convergence with respect to mesh size: (a) base pressure; (b) pressure convergence

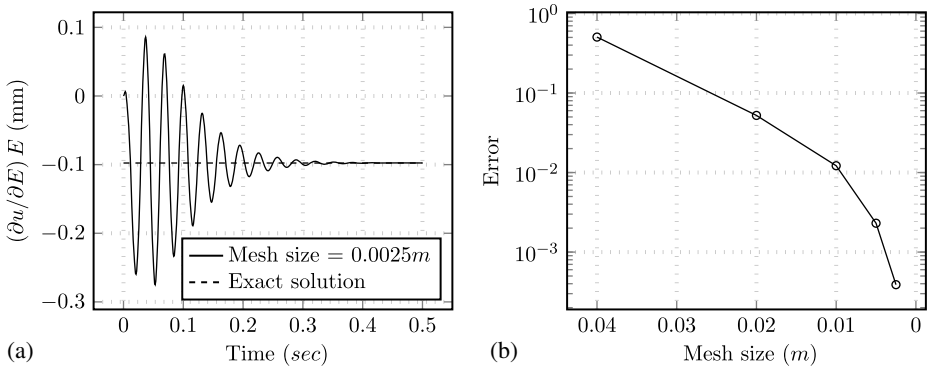

Fig. 5. Sensitivity of tip node displacement with respect to beam elastic modulus and convergence with respect to mesh size: (a) scaled displacement sensitivity to E; (b) displacement sensitivity convergence

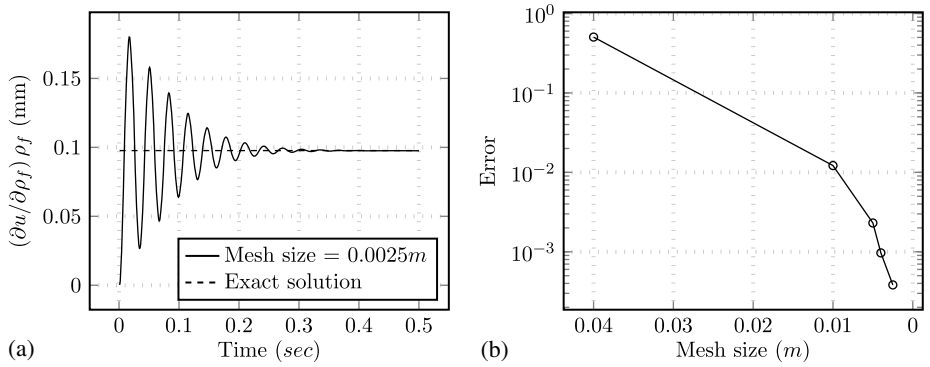

Fig. 6. Sensitivity of tip node displacement with respect to fluid density and convergence with respect to mesh size: (a) scaled displacement sensitivity to ρ_f; (b) displacement sensitivity convergence

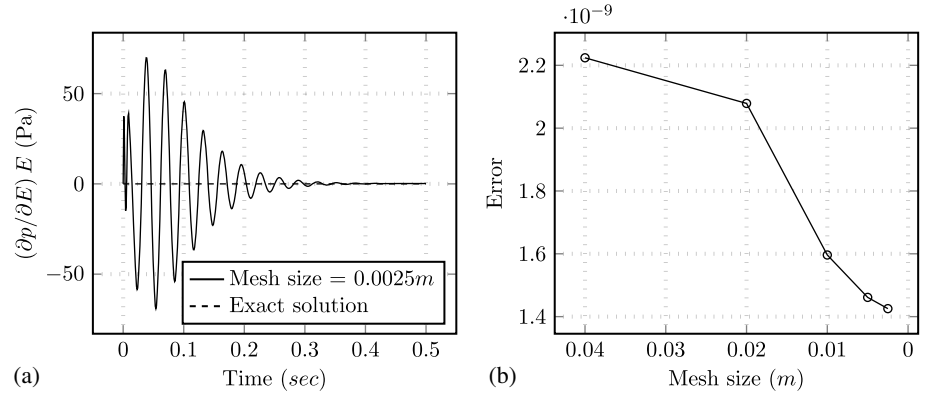

Fig. 7. Sensitivity of base node pressure with respect to beam elastic modulus and convergence with respect to mesh size: (a) scaled pressure sensitivity to E; (b) pressure sensitivity convergence

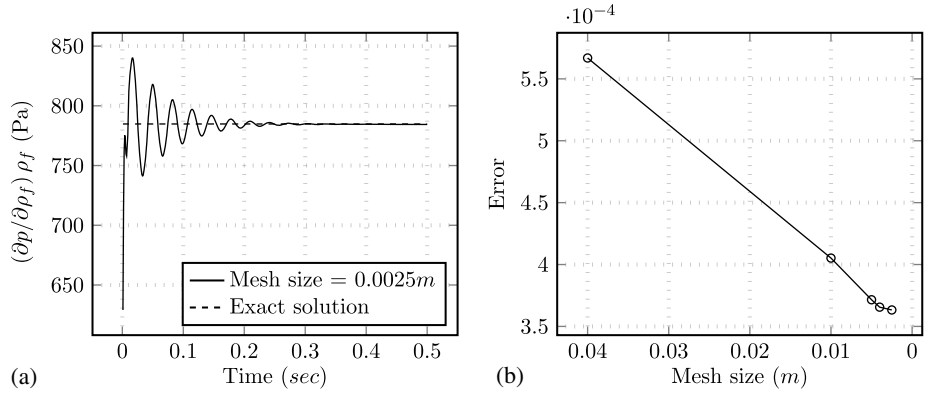

Fig. 8. Sensitivity of base node pressure with respect to fluid density and convergence with respect to mesh size: (a) scaled pressure sensitivity to ρ_f; (b) pressure sensitivity convergence

Hydrostatic Loading on a Beam

A classic problem in structural analysis is solving for the deflection of a beam subjected to hydrostatic pressure. With a closed-form solution in the small displacement, linear-elastic range, this represents a suitable problem to verify the DDM sensitivity implementation prior to examining simulations with material and geometric nonlinear structural response.

The model for this example, shown in Fig. 2(a), is an open tank with fixed boundaries on the left and bottom and a flexible beam on the right. The fluid depth is $h = 0.08$ m while the beam length is $L = 0.1$ m. Using the structural analysis model shown in Fig. 2(b), the horizontal deflection at the free end of the beam is

$$u = \frac{w}{EI}\left[\frac{h^4}{30} + (L-h)\frac{h^3}{24}\right] \tag{78}$$

where $E = 100$ MPa is the elastic modulus of the beam. The second moment of the beam cross-sectional area, I, is computed from the section width, $b = 0.012$ m, and section depth, $d = 0.012$ m.

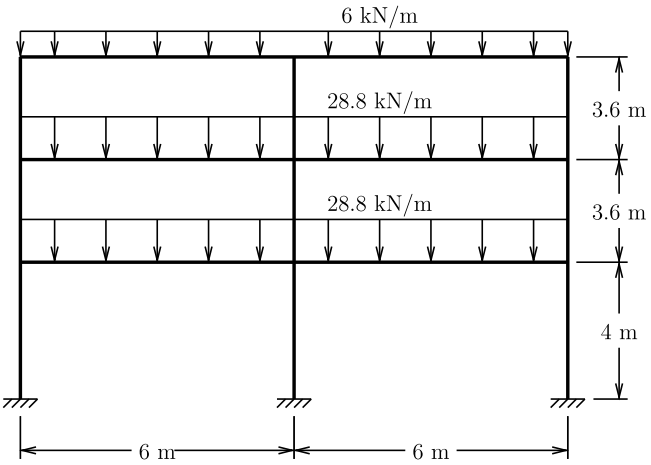

Fig. 9. Geometry and floor loads of reinforced-concrete frame example

The peak intensity of distributed loading on the beam, w, is equal to the beam width multiplied by the peak hydrostatic pressure, $p = \rho_f gh$

$$w = (\rho_f gh)b \tag{79}$$

where the fluid density $\rho_f = 1{,}000$ kg/m^3; and the gravitational constant is $g = 9.81$ m/s^2. The out-of-plane thickness of the fluid domain is assumed equal to the beam width, b. Using the given numerical values, the peak hydrostatic pressure at the base of the beam is $p = 784.8$ Pa, leading to a peak distributed load of $w = 9.418$ N/m according to Eq. (79), and a static deflection of $u = 0.09767$ mm from Eq. (78). The density of the beam is $\rho_s = 2{,}500$ kg/m^3.

Time histories of the beam deflection and base pressure are shown in Figs. 3 and 4, wherein the simulated responses reach a steady state about the known static solutions and converge as the fluid and beam mesh sizes decrease. The ensuing time histories of response sensitivity with respect to beam modulus, E, and fluid

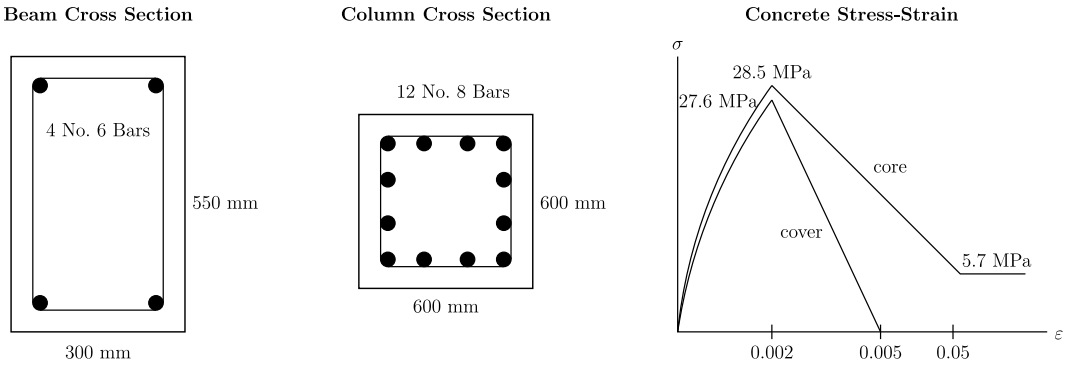

Fig. 10. Beam and column cross-sections of reinforced-concrete frame

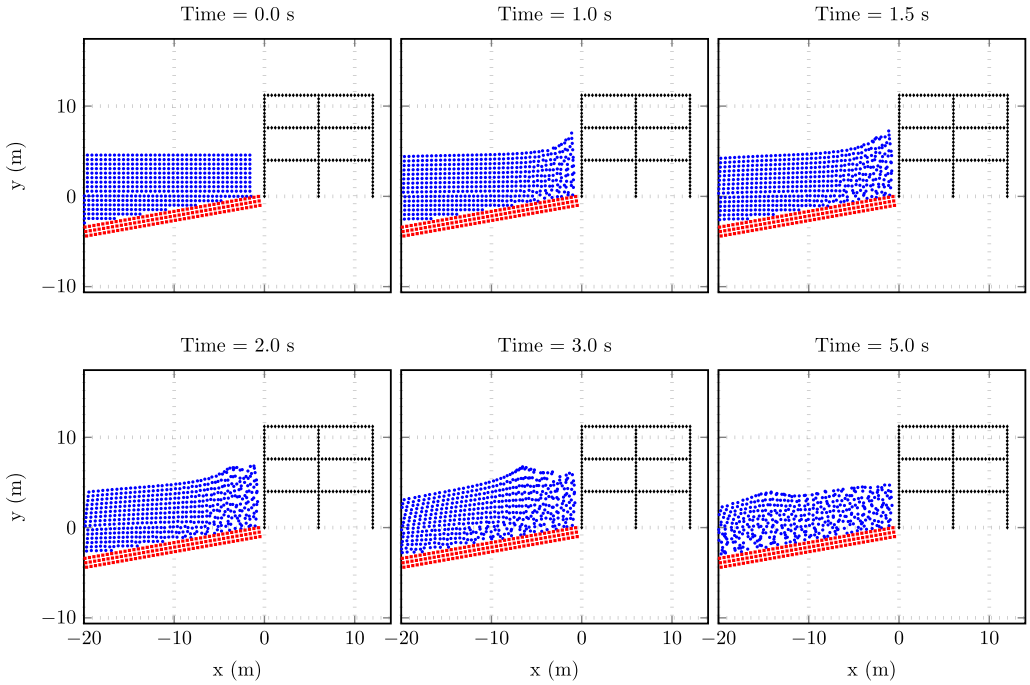

Fig. 11. Snap shots of the tsunami runup on coastal structure

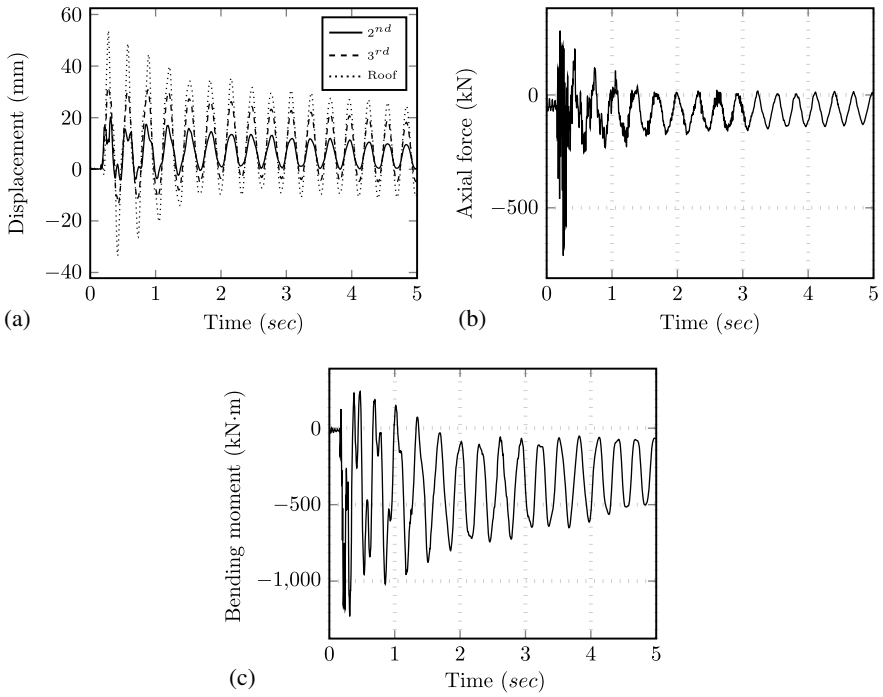

Fig. 12. Floor displacements and axial force and bending moment at the base of right column: (a) floors' displacements; (b) base axial forces; (c) base bending moments

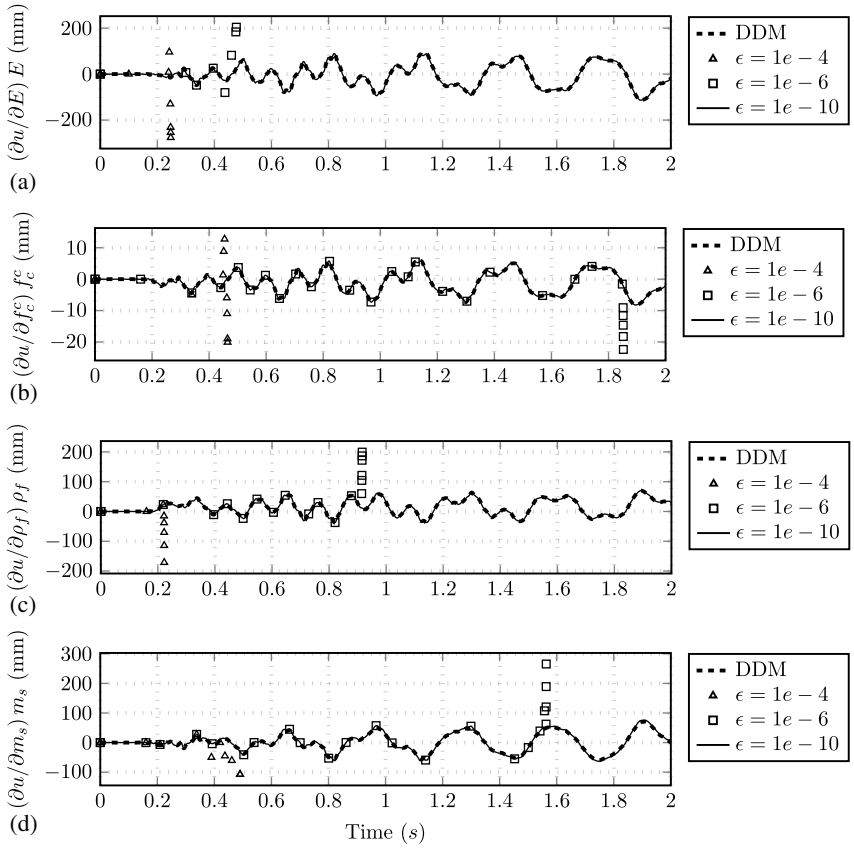

Fig. 13. Sensitivity of second-floor displacement with respect to steel elastic modulus, column concrete compressive strength, fluid density, and structural mass computed by DDM and FDM: (a) scaled displacement sensitivity to E; (b) scaled displacement sensitivity to f_c^c; (c) scaled displacement sensitivity to ρ_f; (d) scaled displacement sensitivity to m_s

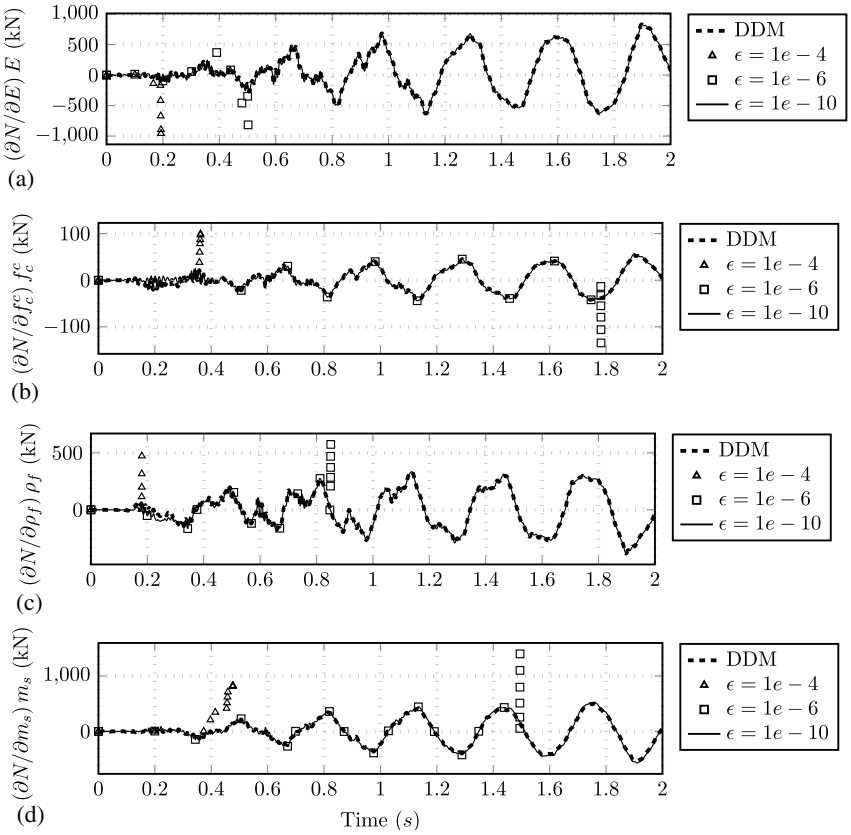

Fig. 14. Sensitivity of axial force at the base of right column with respect to steel elastic modulus, column concrete compressive strength, fluid density, and structural mass computed by DDM and FDM: (a) scaled axial force sensitivity to E; (b) scaled axial force sensitivity to f_c^c; (c) scaled axial force sensitivity to ρ_f; (d) scaled axial force sensitivity to m_s

density, ρ_f, are computed for the beam deflection and base pressure. The derivatives of the exact solution of deflection are scaled by the parameter value as follows:

$$E\frac{\partial u}{\partial E} = -u, \qquad \rho_f \frac{\partial u}{\partial \rho_f} = u \tag{80}$$

As shown in Fig. 5, the sensitivity of the tip deflection to E converges to the expected derivative of the static solution as the fluid and beam mesh sizes decrease. The sensitivity is negative because the deflection will decrease if E increases, making the beam stiffer. Similarly, the deflection sensitivity with respect to fluid density, ρ_f, is positive as this parameter corresponds to the loading applied to the beam as shown in Fig. 6. For the sensitivities of pressure shown in Fig. 7, the computed solutions reach the steady-state solution of zero as the hydrostatic pressure does not depend on the beam properties. The scaled pressure sensitivity to fluid density converges to the expected solution, $\rho_f(\partial p/\partial \rho_f) = p$, as shown in Fig. 8.

Tsunami Impact on Coastal Structure

This example is of a tsunami bore impacting a three-story reinforced-concrete building. The structural model shown in Fig. 9 was adapted from Madurapperuma and Wijeyewickrema (2012) for the analysis of water-borne debris and was further analyzed by Zhu and Scott (2014b) to demonstrate fluid–structure interaction using the PFEM. To capture material and geometric nonlinearity, each frame member is discretized in to 10 displacement-based beam–column finite-elements (*dispBeamColumn* in *OpenSees*) with fiber-discretized cross sections at the element integration points and the corotational geometric transformation (Crisfield 1991). The refined mesh of beam elements also prevents fluid from passing through the frame members, indicative of a closed first story. DDM sensitivity for the frame elements is described in Scott et al. (2004) while that for the corotational transformation is provided in Scott and Filippou (2007).

The cross-section dimensions, reinforcing details, and concrete properties of the frame are shown in Fig. 10. Light transverse reinforcement provides residual concrete compressive strength in the core regions of the members. Zero tensile strength is assumed for the concrete (*Concrete01* in *OpenSees*) and the longitudinal reinforcing steel is assumed bilinear with elastic modulus 200 GPa, yield strength 420 MPa, and 1% kinematic strain hardening (*Steel01* in *OpenSees*). Gravity loads and nodal mass were calculated assuming uniform pressure of 4.8 kPa on floor slabs and 1.0 kPa on the roof with a tributary width of 3 m.

The tsunami bore has a height of 4 m, initial velocity of 2 m/s, and out-of-plane thickness of 3 m. The simulation begins at impending impact of the frame and the response at various snapshots is shown in Fig. 11. The floor displacements and the axial forces and the bending moment at the base of the right-most first-floor column are shown in Fig. 12.

Sensitivity time histories of the roof displacement, axial force, and bending moment computed by the DDM are compared to FDM results with respect to the steel elastic modulus, E; column concrete compressive strength, f_c^c; fluid density, ρ_f; and structural mass, m_s as shown in Figs. 13–15. Due to high-frequency response for pressures and their contributions to stress and force recovery, the results for the axial force and bending moment sensitivity computed by the DDM and FDM have been smoothed with the same algorithm.

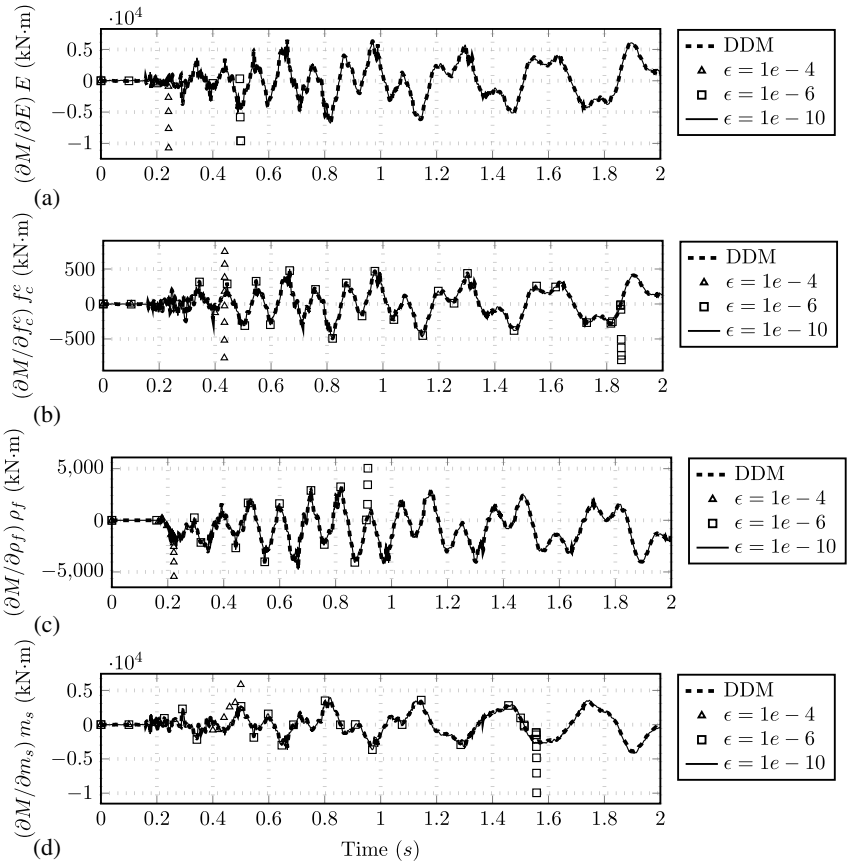

Fig. 15. Sensitivity of bending moment at the base of right column with respect to steel elastic modulus, column concrete compressive strength, fluid density, and structural mass computed by DDM and FDM: (a) scaled bending moment sensitivity to E; (b) scaled bending moment sensitivity to f_c^c; (c) scaled bending moment sensitivity to ρ_f; (d) scaled bending moment sensitivity to m_s

Regardless of smoothing, as the parameter perturbations decrease, the finite-difference approximation should converge to the DDM result, thereby verifying the DDM implementation

$$\lim_{\Delta\theta \to 0} \frac{\Delta U}{\Delta \theta} = \frac{\partial U}{\partial \theta} \tag{81}$$

Figs. 13–15 show that the DDM matches the smallest finite-difference perturbation, $\varepsilon = 10^{-10}$, where $\varepsilon = \Delta\theta/\theta$. For the larger parameter perturbations such as $\varepsilon = 10^{-4}$ and $\varepsilon = 10^{-6}$, the figures show sudden jumps in the finite-difference results. These jumps are due to remeshing of the fluid domain at every time step, where ultimately the finite-difference approach breaks down because it compares response quantities from two different meshes. The figures show that smaller parameter perturbations tend to postpone the divergence of the finite-difference approximations to later in the simulation. Although it provides a useful verification tool, the FDM is not a reliable approach for gradient-based problems involving FSI simulations based on the PFEM.

Conclusion

The PFEM is an effective approach to simulating FSI because it uses a Lagrangian formulation for the fluid domain, which is the same formulation typically employed for finite-element analysis of structures. The development of DDM sensitivity equations for the PFEM broaden its application to gradient-based algorithms in structural reliability, optimization, and system identification of FSI as well as other application spaces of the PFEM including thermo-mechanical analysis and fluid–soil–structure interaction (Marti et al. 2012; Oñate et al. 2011). Due to geometric nonlinearity of the fluid domain, additional terms were required to derive and implement the DDM equations for the PFEM. Following the same analysis procedure as for the response itself, the sensitivity equations are solved using the fractional step method (FSM). The sensitivity equations were verified using closed-form solutions for the classic problem of hydrostatic loading on a beam and shown to match finite-difference solutions with decreasing parameter perturbations for tsunami loading on a reinforced-concrete frame. It was also shown that the finite-difference approach to computing sensitivity is not applicable to the PFEM because the finite-element mesh of the fluid domain changes throughout a simulation. Future applications of DDM sensitivity for the PFEM include time variable reliability analysis of fluid–structure interaction, which is an important consideration for multihazard analysis involving wind loading concurrent with storm surge and tsunami following an earthquake.

Acknowledgments

This material is based on work supported by the National Science Foundation under Grant No. 0847055. Any opinions, findings, and conclusions or recommendations expressed in this material are those of the authors and do not necessarily reflect the views of the National Science Foundation.

References

Arnold, D., Brezzi, F., and Fortin, M. (1984). "A stable finite element for the Stokes equations." *Math. Stat.*, 21(4), 337–344.

Baiges, J., and Codina, R. (2010). "The fixed-mesh ale approach applied to solid mechanics and fluid-structure interaction problems." *Int. J. Numer. Meth. Eng.*, 81(2), 1529–1557.

Bank, R. E. and Welfert, B. D. (1990). "A comparison between the mini-element and the Petrov-Galerkin formulations for the generalized stokes problem." *Comput. Meth. Appl. Mech. Eng.*, 83(1), 61–68.

Bebamzadeh, A., Haukaas, T., Vaziri, R., Poursartip, A., and Fernlund, G. (2010). "Application of response sensitivity in composite processing." *J. Compos. Mater.*, 44(15), 1821–1840.

Brezzi, F., and Fortin, M. (1991). *Mixed and hybrid finite element methods*, Springer, New York.

Chock, G., Carden, L., Robertson, I., Olsen, M., and Yu, G. (2013). "Tohoku tsunami-induced building failure analysis with implications for U.S. tsunami and seismic design codes." *Earthquake Spectra*, 29(S1), S99–S126.

Chock, G. Y. K., Robertson, I., and Riggs, H. R. (2011). "Tsunami structural design provisions for a new update of building codes and performance-based engineering." *ASCE solutions of coastal disasters (COPRI)*, Anchorage, AK, 423–435.

Conte, J. P., Barbato, M., and Spacone, E. (2004). "Finite element response sensitivity analysis using force-based frame models." *Int. J. Numer. Meth. Eng.*, 59(13), 1781–1820.

Conte, J. P., Vijalapura, P. K., and Meghalla, M. (2003). "Consistent finite-element response sensitivity analysis." *J. Eng. Mech.*, 10.1061/(ASCE)0733-9399(2003)129:12(1380), 1380–1393.

Crisfield, M. A. (1991). *Non-linear finite element analysis of solids and structures*, Vol. 1, Wiley, Chichester, U.K.

Donea, J., and Huerta, A. (2003). *Finite element methods for flow problems*, Wiley, Chichester, U.K.

Franchin, P. (2004). "Reliability of uncertain inelastic structures under earthquake excitation." *J. Eng. Mech.*, 10.1061/(ASCE)0733-9399(2004)130:2(180), 180–191.

Fujimura, K., and Kiureghian, A. D. (2007). "Tail-equivalent linearization method for nonlinear random vibration." *Probab. Eng. Mech.*, 22(1), 63–76.

Girault, V., and Raviart, P. (1986). *Finite element methods for Navier-Stokes equations*, Springer, Berlin.

Gresho, P. M. (1998). *Incompressible flow and the finite element method: Advection-diffusion and isothermal laminar flow*, Wiley, Chichester, U.K.

Gu, Q., Barbato, M., Conte, J. P., Gill, P., and McKenna, F. (2012). "OpenSees-SNOPT framework for finite-element-based optimization of structural and geotechnical systems." *J. Struct. Eng.*, 10.1061/(ASCE)ST.1943-541X.0000511, 822–834.

Gunzburger, M. (1989). *Finite element methods for viscous incompressible flows*, Academic Press, San Diego.

Guo, Q. and Jeffers, A. E. (2014). "Direct differentiation method for response sensitivity analysis of structures in fire." *Eng. Struct*, 77, 172–180.

Haukaas, T., and Scott, M. H. (2006). "Shape sensitivities in the reliability analysis of nonlinear frame structures." *Comput. Struct.*, 84(15–16), 964–977.

Kleiber, M., Antunez, H., Hien, T., and Kowalczyk, P. (1997). *Parameter sensitivity in nonlinear mechanics*, Wiley, Chichester, U.K.

Lee, M., Chung, S., Jang, S., and Joun, M. (2009). "Three-dimensional simulation of forging using tetrahedral and hexahedral elements." *Finite Elem. Anal. Des.*, 45(11), 745–754.

Madurapperuma, M. A. K. M., and Wijeyewickrema, A. C. (2012). "Inelastic dynamic analysis of an RC building impacted by a tsunami waterborne shipping container." *J. Earthquake Tsunami*, 6(1), 1250001.

Marti, J., Ryzhakov, P., Idelsohn, S., and Oñate, E. (2012). "Combined Eulerian—PFEM approach for analysis of polymers in fire situations." *Int. J. Numer. Meth. Eng.*, 92(9), 782–801.

Matsumoto, J. (2005). "A relationship between stabilized fem and bubble function element stabilization method with orthogonal basis for incompressible flows." *J. Appl. Mech.*, 8, 233–242.

McAllister, T. (2014). "The performance of essential facilities in Superstorm Sandy." *ASCE Structures Congress*, ASCE, Reston, VA, 2269–2281.

Nakajima, S., and Kawahara, M. (2010). "New finite element formulation based on bubble function interpolation for the transient compressible euler equations." *Int. J. Numer. Meth. Biomed. Eng.*, 26(8), 1030–1049.

Oñate, E., Celigueta, M., Idelsohn, S., Salazar, F., and Suárez, B. (2011). "Possibilities of the particle finite element method for fluid–soil–structure interaction problems." *Comput. Mech.*, 48(3), 307–318.

Oñate, E., García, J., Idelsohn, S., and Pin, F. D. (2006). "Finite calculus formulations for finite element analysis of incompressible flows. Eulerian, ALE and Lagrangian approaches." *Comput. Meth. Appl. Mech. Eng.*, 195(23–24), 3001–3037.

Oñate, E., Idelsohn, S., Pin, F. D., and Aubry, R. (2004). "The particle finite element method. an overview." *Int. J. Comput. Meth.*, 1(2), 267–307.

OpenSees version 2.4.6 [Computer software]. UC regents, Berkeley, CA.

Pierre, R. (1995). "Optimal selection of the bubble function in the stabilization of the P1-P1 element for the Stokes problem." *SIAM J. Numer. Anal.*, 32(4), 1210–1224.

Radovitzky, R., and Ortiz, M. (1998). "Lagrangian finite element analysis of Newtonian fluid flows." *Int. J. Numer. Meth. Eng.*, 43(4), 607–619.

Scott, M. H., and Filippou, F. C. (2007). "Exact response gradients for large displacement nonlinear beam-column elements." *J. Struct. Eng.*, 10.1061/(ASCE)0733-9445(2007)133:2(155), 155–165.

Scott, M. H., Franchin, P., Fenves, G. L., and Filippou, F. C. (2004). "Response sensitivity for nonlinear beam-column elements." *J. Struct. Eng.*, 10.1061/(ASCE)0733-9445(2004)130:9(1281), 1281–1288.

Scott, M. H., and Haukaas, T. (2008). "Software framework for parameter updating and finite-element response sensitivity analysis." *J. Comput. Civ. Eng.*, 10.1061/(ASCE)0887-3801(2008)22:5(281), 281–291.

Tezduyar, T., Mittal, S., Ray, S., and Shih, R. (1992). "Incompressible flow computations with stabilized bilinear and linear equal-order-interpolation velocity-pressure elements." *Comput. Meth. Appl. Mech. Eng.*, 95(2), 221–242.

Zhu, M., and Scott, M. H. (2014a). "Improved fractional step method for simulating fluid-structure interaction using the pfem." *Int. J. Numer. Meth. Eng.*, 99(12), 925–944.

Zhu, M., and Scott, M. H. (2014b). "Modeling fluid-structure interaction by the particle finite element method in OpenSees." *Comput. Struct.*, 132, 12–21.

Zienkiewicz, O., Taylor, R., and Zhu, J. (2005). *The finite element method: Its basis and fundamentals*, 6th Ed., Vol. 1, Elsevier Butterworth-Heinemann, Oxford, U.K.